Journal of Sound and Vibration (2002) **252**(3), 389–408
doi:10.1006/jsvi.2001.3910, available online at http://www.idealibrary.com on IDEAL®

ANALYSIS OF THE MULTIPLE-SOLUTION RESPONSE OF A FLEXIBLE ROTOR SUPPORTED ON NON-LINEAR SQUEEZE FILM DAMPERS

C. S. Zhu

Department of Electrical Engineering, Zhejiang University, 310027, *Hangzhou, Zhejiang, People's Republic of China. E-mail: cszhu@hotmail.com*

AND

D. A. Robb and D. J. Ewins

Centre of Vibration Engineering, Department of Mechanical Engineering, Imperial College of Science, Technology and Medicine, London SW7 2BX, England

(*Received* 15 *June* 2000, *and in final form* 25 *June* 2001)

The multiple-solution response of rotors supported on squeeze film dampers is a typical non-linear phenomenon. The behaviour of the multiple-solution response in a flexible rotor supported on two identical squeeze film dampers with centralizing springs is studied by three methods: synchronous circular centred-orbit motion solution, numerical integration method and slow acceleration method using the assumption of a short bearing and cavitated oil film; the differences of computational results obtained by the three different methods are compared in this paper. It is shown that there are three basic forms for the multiple-solution response in the flexible rotor system supported on the squeeze film dampers, which are the resonant, isolated bifurcation and swallowtail bifurcation multiple solutions. In the multiple-solution speed regions, the rotor motion may be subsynchronous, super-subsynchronous, almost-periodic and even chaotic, besides synchronous circular centred, even if the gravity effect is not considered. The assumption of synchronous circular centred-orbit motion for the journal and rotor around the static deflection line can be used only in some special cases; the steady state numerical integration method is very useful, but time consuming. Using the slow acceleration method, not only can the multiple-solution speed regions be detected, but also the non-synchronous response regions.

1. INTRODUCTION

It is well known that the squeeze film damper, which is used in the rotor support structures of aero-engines to control rotor vibration and transmitted force through the bearings, behaves non-linearly in the region of high journal eccentricity ratios. Various non-linear phenomena can be observed experimentally in rotor systems supported on squeeze film dampers; the multiple solution in the imbalanced response curves is a typical non-linear phenomenon. Generally, the largest and the smallest solutions are stable; this phenomenon is often called bistable operation in squeeze film damper research. Since the largest solution of the bistable operation, characterized by the large vibration amplitude and transmitted force, has a great influence on the reliability of the damper, a very important problem in the design of squeeze film dampers is to determine the regions and locations of multiple solutions and to analyse the behaviour of the rotor systems.

0022-460X/02/$35.00

Many methods, for example, synchronous circular centred-orbit motion solution [1–5], harmonic balance method [6, 7], trigonometric collocation method [8], generalized polynomial expansion method [9], numerical integration method [10, 11], etc., have been used to analyse the dynamic behaviour of non-linear rotor systems, but there are some advantages and limitations for every analysis method mentioned above. The synchronous circular centred-orbit motion solution can be used to get the steady state solutions only in some special cases even if a centralizing spring is used in parallel with the squeeze film damper or the rotor is mounted vertically. The main disadvantages of the harmonic balance method, trigonometric collocation method, and generalized polynomial expansion method are that it is difficult to choose fundamental frequency and to obtain all possible solutions by numerical iterative schemes. The numerical integration method is able to predict the steady state and the transient response, either synchronous or non-synchronous, and even chaotic motions, but it is time-consuming and difficult to select the initial conditions for convergence to all possible solutions.

In this paper, the behaviour of the multiple solution in a flexible rotor–squeeze film damper is analysed by the synchronous circular centred-orbit motion solution, numerical integration method and slow acceleration method, and the computational results from the three different methods are compared. In order to reduce the complex mathematical problems in obtaining all solutions of multiple-variable non-linear equations, a symmetrical Jeffcott rotor supported on two identical squeeze film dampers with centralizing springs is chosen and with the assumption that the short bearing and cavitation oil film model are applicable.

2. ROTOR MODEL AND ANALYSIS METHODS

2.1. ROTOR MODEL

The rotor system to be investigated is a Jeffcott rotor symmetrically supported on two identical squeeze film dampers with the centralizing springs as shown in Figure 1(a). O_B is the geometric centre of the journal. O_m is the gravity centre of the disc, and O_D is the geometric centre of the disc. In order to simplify the analysis, the following assumptions are made:

(a) the rotor is symmetric and supported on two identical dampers with the same parameters;
(b) the imbalance of the rotor system is defined at the mid-plane of the rotor and the rotor mass is lumped at the rotor mid-plane and at the two damper stations;
(c) the rotor stiffness and the centralizing spring stiffness are radially symmetric and the damping at the mid-span disc due to the aerodynamic effect is viscous;
(d) the gyroscopic effect of the disc on the rotor system is neglected due to the symmetry;
(e) the axial and torsional vibrations of the rotor system and the influence of the rolling element bearings are negligible;
(f) the rotor is centrally preloaded with constant radial support stiffness, the effect of the gravity is neglected;
(g) the oil film forces of the damper are determined by the Reynolds equation with an incompressible lubricant, and the short bearing and cavitated π-film are applicable.

Since the rotor system is symmetric about its mid-span, it is sufficient to consider one-half of the system only. Thus, the equations of motion of the rotor system in Cartesian

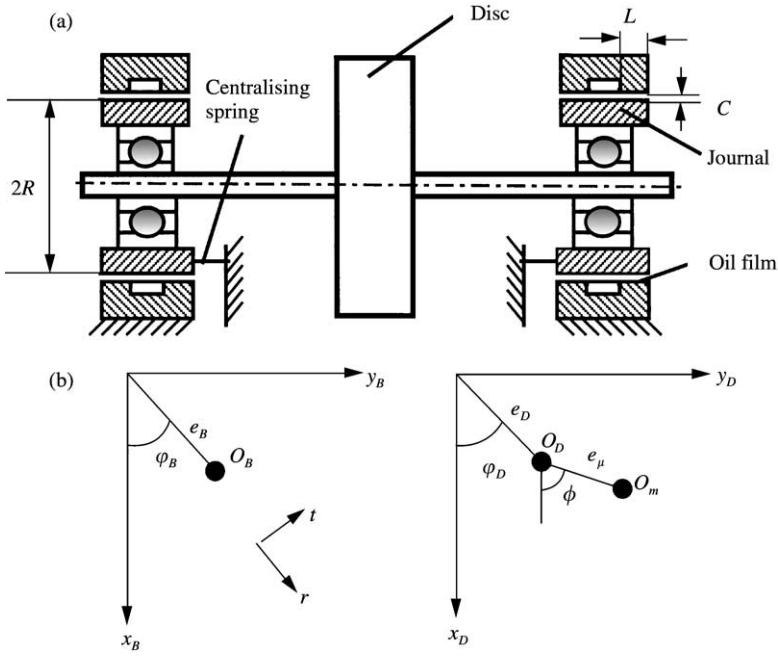

Figure 1. Flexible rotor–squeeze film damper model and co-ordinate system.

co-ordinates in Figure 1(b) can be expressed in varying speed operation as

$$m_D\ddot{x}_D + c_D\dot{x}_D + k_S(x_D - x_B) = m_D e_\mu(\dot{\phi}_D^2\cos\phi_D + \ddot{\phi}_D\sin\phi_D),$$
$$m_D\ddot{y}_D + c_D\dot{y}_D + k_S(y_D - y_B) = m_D e_\mu(\dot{\phi}_D^2\sin\phi_D - \ddot{\phi}_D\cos\phi_D), \tag{1}$$
$$m_B\ddot{x}_B + \frac{k_S}{2}(x_B - x_D) + \frac{k_a}{2}x_B = F_x, \qquad m_B\ddot{y}_B + \frac{k_S}{2}(y_B - y_D) + \frac{k_a}{2}y_B = F_y,$$

where k_s is the stiffness of the shaft, k_a is the stiffness of the centralizing spring, m_D and m_B are the lumped masses at the disc and the journal positions, c_D is the viscous damping coefficient of the disc due to aerodynamic effect, F_x and F_y are oil film forces generated by the squeeze film damper in the x- and y-direction, respectively, (x_D, y_D) and (x_B, y_B) are displacements of the disc and the journal in the fixed co-ordinate system, respectively, e_μ is the mass imbalance eccentricity of the disc, ϕ_D is the attitude angle of the disc imbalance force vector with respect to the x axial direction and $(\cdot)$ denotes $\mathrm{d}/\mathrm{d}t$.

Let $\mathbf{z}_B = x_B + \mathrm{i}y_B = e_B\mathrm{e}^{\mathrm{i}\varphi_B}$ and $\mathbf{z}_D = x_D + \mathrm{i}y_D = e_D\mathrm{e}^{\mathrm{i}\varphi_D}$, e_B and e_D are journal and disc eccentric displacements from the static deflection line; equation (1) can also be expressed in complex variable $\mathbf{z}$ as

$$m_D\ddot{z}_D + c_D\dot{z}_D + k_S(\mathbf{z}_D - \mathbf{z}_B) = m_D e_\mu(\dot{\phi}_D^2\,\mathrm{e}^{\mathrm{i}\phi_D} - \mathrm{i}\ddot{\phi}_D\,\mathrm{e}^{-\mathrm{i}\phi_D}), \tag{2}$$

$$m_B\ddot{z}_B + \frac{k_s}{2}(\mathbf{z}_B - \mathbf{z}_D) + \frac{k_a}{2}\mathbf{z}_B = (F_x + \mathrm{i}F_y). \tag{3}$$

Dividing equations (2) and (3) by $m_D\omega_r^2 C$ and $m_B\omega_r^2 C$, respectively, and defining a non-dimensional time $\tau = \omega_r t$, ω_r is a reference rotational speed, the non-dimensional equations

of motion of the rotor system are given by

$$\mathbf{Z}_D'' + \frac{2\xi\Omega_r}{\Omega}\mathbf{Z}_D' + \Omega_r^2/\Omega^2\,(\mathbf{Z}_D - \mathbf{Z}_B) = U(\phi_D'^2\,\mathrm{e}^{\mathrm{i}\phi_D} - \mathrm{i}\phi_D''\,\mathrm{e}^{-\mathrm{i}\phi_D}), \tag{4}$$

$$\mathbf{Z}_B'' + \frac{\Omega_r^2}{2\alpha\Omega^2}(\mathbf{Z}_B - \mathbf{Z}_D) + \frac{k\Omega_r^2}{2\alpha\Omega^2}\mathbf{Z}_B = \frac{\Omega_r}{\Omega}(\bar{F}_x + \mathrm{i}\bar{F}_y), \tag{5}$$

where $\mathbf{Z}_B = \varepsilon_B \mathrm{e}^{\mathrm{i}\varphi_B}$ and $\mathbf{Z}_D = \varepsilon_B\,\mathrm{e}^{\mathrm{i}\varphi_D}$; $\varepsilon_B = e_B/C$ and $\varepsilon_D = e_D/C$ are the journal and disc eccentricity ratios, ($''$) denotes $\mathrm{d}^2/\mathrm{d}\tau^2$, C is the radial clearance of the damper, $\alpha = m_B/m_D$ is the mass ratio, $\xi = c_D/2m_D\omega_{cr}$ is the damping ratio, $k = k_a/k_s$ is the stiffness ratio, $U = e_\mu/C$ is the imbalance parameter of the rotor system, $\Omega = \omega/\omega_{cr}$ is the rotational speed ratio, $\Omega_r = \omega/\omega_r$ is the reference rotational speed ratio, ω is the rotational speed of the rotor system, ω_{cr} is the first pin–pin critical speed of the flexible rotor mounted rigidly, $\bar{F}_x$ and $\bar{F}_y$, are the non-dimensional oil film force components of the squeeze film damper in the x- and y-direction, respectively, which depend on the oil film model used in the theoretical analysis.

The squeeze film damper can be simply an annular fluid-filled space surrounding the out race of a rolling element bearing. The oil film forces in the x- and y-direction, F_x and F_y, are obtained from the oil film pressure distribution, which is obtained from the Reynolds equation. For the squeeze film damper, the Reynolds equation can be written in the following form:

$$\frac{1}{R^2}\frac{\partial}{\partial\theta}\left(h^3\frac{\partial p}{\partial\theta}\right) + \frac{\partial}{\partial z}\left(h^3\frac{\partial p}{\partial z}\right) = -12\,\omega\mu\,(\dot{\varepsilon}_B\cos\theta + \varepsilon_B\dot{\varphi}_B\sin\theta), \tag{6}$$

where R is the journal radius of the damper, $h = C(1 + \varepsilon_B\cos\theta)$ is the oil film thickness in the position θ, p is the oil film pressure, μ is the viscosity of the fluid, θ is the position angle of the journal measured from line to centres. Note that equation (6) implies constant fluid properties and incompressible laminar flow, and neglects the effect of the fluid inertia and the curvature of journal and damper surfaces.

For a squeeze film damper without side-seals and $L/D < 0{\cdot}25$, the variation of the oil film pressure in the circumferential direction is smaller than that in the axial direction, so the first term about $\partial p/\partial\theta$ in equation (6) can be omitted, resulting in the short bearing approximation. For the short bearing approximation, atmospheric supply and end pressures, and no misalignment of the journal, the oil film pressure of the squeeze film damper is [12]

$$p(\theta, z) = -6\mu C/h^3\left(\frac{L^2}{4} - z^2\right)(\dot{\varepsilon}_B\cos\theta + \varepsilon_B\dot{\varphi}_B\sin\theta). \tag{7}$$

The oil film forces of the squeeze film damper about the damper centre in the radial and tangential directions are obtained by integrating the oil film pressure distribution along and normal to the line of the centres of the journal over a certain region as

$$\begin{pmatrix} F_r \\ F_t \end{pmatrix} = 2\int_{-L/2}^{L/2}\int_{\theta_1}^{\theta_2} p(\theta, z)\,RL\begin{pmatrix}\sin\theta\\ \cos\theta\end{pmatrix}\mathrm{d}\theta\,\mathrm{d}z. \tag{8}$$

The integrating region θ_1 and θ_2 will be determined by the oil film cavitational boundary condition. Since the journal of the damper does not always operate in a circular motion, it means that $\mathrm{d}\varepsilon_B/\mathrm{d}t = \dot{\varepsilon}_B$ is generally not equal to zero, so the oil film limits, θ_1 and θ_2, should

taken to lie at the circumferential points where p becomes zero. Thus θ_1 and θ_2 are found by equating the right-hand side of equation (7) to zero, giving

$$\theta_1 = \tan^{-1}(-\dot{\varepsilon}_B/\varepsilon_B\dot{\varphi}_B) \quad \text{and} \quad \theta_2 = \theta_1 + \pi. \tag{9}$$

Therefore, one has

$$F_r = -\frac{2\mu RL^3}{C^2}[\varepsilon_B\dot{\varphi}_B I_3^{11} + \dot{\varepsilon}_B I_3^{02}] = -\frac{2\mu RL^3}{C^2} f_r,$$

$$F_t = -\frac{2\mu RL^3}{C^2}[\varepsilon_B\dot{\varphi}_B I_3^{20} + \dot{\varepsilon}_B I_3^{11}] = -\frac{2\mu RL^3}{C^2} f_t, \tag{10}$$

where

$$I_k^{mn} = \int_{\theta_1}^{\theta_2} \frac{\sin^m\theta\cos^n\theta}{(1+\varepsilon_B\cos\theta)^k}\,\mathrm{d}\theta, \ (k, m \text{ and } n \text{ are 0, 1, 2, or 3})$$

is the bearing integral, which can be obtained from the Sommerfeld transform or Booker integral table [13]. Finally, one has the non-dimensional oil film force components in the xy-co-ordinate system as

$$\bar{F}_x = -\frac{2B}{\sqrt{(X_B^2 + Y_B^2)}}[X_B(\varepsilon_B\varphi'_B I_3^{11} + \varepsilon'_B I_3^{02}) - Y_B(\varepsilon_B\varphi'_B I_3^{20} + \varepsilon'_B I_3^{11})] = -2Bf_x, \tag{11}$$

$$\bar{F}_y = -\frac{2B}{\sqrt{(X_B^2 + Y_B^2)}}[Y_B(\varepsilon_B\varphi'_B I_3^{11} + \varepsilon'_B I_3^{02}) + X_B(\varepsilon_B\varphi'_B I_3^{20} + \varepsilon'_B I_3^{11})] = -2Bf_y. \tag{12}$$

2.2. ANALYSIS METHODS

2.2.1. *Synchronous circular centred-orbit motion solution*

For a rotor system supported on the squeeze film damper with a centralizing spring, the centralizing spring is used to centrally pre-load the rotor system; the assumption of the synchronous circular centred-orbit (CCO) motion of the rotor around the undeformed line in the steady state at the same frequency of the rotational speed is often used in squeeze film damper research [1–5].

For the synchronous circular centred-orbit motion, let $\omega_r = \omega$ and $\phi_D = \tau = \omega t$. As $\mathbf{Z}_B = \varepsilon_B e^{i\varphi_B}$ and $\mathbf{Z}_D = \varepsilon_D e^{i\varphi_D}$, the conditions for the synchronous circular centred-orbit solution are $\varepsilon''_D = \varepsilon'_D = 0$, $\varphi''_D = 0$, and $\varphi'_D = 1$, one has $\varepsilon_D = \varepsilon_{DO} =$ constant and $\varphi_D = \tau - \phi_{DO}$, where $\phi_{DO} =$ constant, so, $\mathbf{Z}'_D = i\varepsilon_{DO} e^{i(\tau - \phi_{DO})} = i\mathbf{Z}_D$ and $\mathbf{Z}''_D = -\varepsilon_{DO} e^{i(\tau - \phi_{DO})} = -\mathbf{Z}_D$. ϕ_{DO} is the relative phase angle between the disc imbalance force vector and the disc displacement vector. There exist similar results for $\mathbf{Z}_B = \varepsilon_B e^{i\varphi_B}$, where $\varphi_B = \tau - \phi_{BO}$ and $\phi_{BO} =$ constant. In this case, the non-dimensional oil film forces can be obtained from equations (9)–(12).

$$f_r = \frac{2\varepsilon_{BO}}{(1-\varepsilon_{BO}^2)^2}, \quad f_r = \frac{\pi\varepsilon_{BO}}{2(1-\varepsilon_{BO}^2)^{3/2}}, \tag{13}$$

so, equations (4), (5) can be easily transformed to a set of non-linear algebraic equations.

$$\left\{\frac{1+k}{2\alpha\Omega^2}-1-\frac{1-\Omega^2}{2\alpha\Omega^2\,[(1-\Omega^2)^2+(2\xi\Omega)^2]}+\frac{4B}{\Omega}\frac{\varepsilon_{BO}}{(1-\varepsilon_{BO}^2)^2}\right\}^2\varepsilon_{BO}^2$$

$$+\left\{\frac{2\xi\Omega}{2\alpha\Omega^2\,[(1-\Omega^2)^2+(2\xi\Omega)^2]}+\frac{B\pi}{\Omega}\frac{1}{(1-\varepsilon_{BO}^2)^{3/2}}\right\}^2\varepsilon_{BO}^2=\frac{U^2}{4\alpha^2\,[(1-\Omega^2)^2+(2\xi\Omega)^2]},\tag{14}$$

$$\tan\phi_{BO}=\frac{2\xi\Omega\left[\dfrac{1+k}{2\alpha\Omega^2}-1+\dfrac{4B}{\Omega}\dfrac{\varepsilon_{BO}}{(1-\varepsilon_{BO}^2)^2}\right]+\dfrac{\pi B}{\Omega}\dfrac{1-\Omega^2}{(1-\varepsilon_{BO}^2)^{3/2}}}{\left[\dfrac{1+k}{2\alpha\Omega^2}-1+\dfrac{4B}{\Omega}\dfrac{\varepsilon_{BO}}{(1-\varepsilon_{BO}^2)^2}\right](1-\Omega^2)-2\xi\Omega\,\dfrac{\pi B}{\Omega}\dfrac{1}{(1-\varepsilon_{BO}^2)^{3/2}}-\dfrac{1}{2\alpha\Omega^2}}\tag{15}$$

$$\varepsilon_{DO}^2=\frac{(\varepsilon_{BO}\cos\phi_{BO}+U\Omega^2)^2+(\varepsilon_{BO}\sin\phi_{BO})^2}{(1-\Omega^2)^2+(2\xi\Omega)^2}\tag{16}$$

$$\tan\phi_{DO}=\frac{2\xi\Omega\,(\varepsilon_{BO}\cos\phi_{BO}+U\Omega^2)+(1-\Omega^2)\,\varepsilon_{BO}\sin\phi_{BO}}{(1-\Omega^2)(\varepsilon_{BO}\cos\phi_{BO}+U\Omega^2)-2\xi\Omega\varepsilon_{BO}\sin\phi_{BO}}.\tag{17}$$

Equation (14) is a non-linear algebraic equation with only one variable ε_{BO} and because of $0\leqslant\varepsilon_{BO}<1{\cdot}0$, one can easily determine all solutions of the journal eccentricity ratio ε_{BO} by iterative methods, then obtain ϕ_{BO}, ε_{DO} and ϕ_{DO} from equations (15)–(17). Therefore the synchronous circular centred-orbit motion assumption is a very efficient method to analyse the non-linear behaviour of the rotor system with the squeeze film damper and to study the effect of the system parameters on the dynamic behaviour of the rotor system.

2.2.2. *Numerical integration method*

Even if the rotor is mounted vertically or the centralizing spring provides a static load capability to centralize the journal within the radial clearance of the damper in the static state, the assumption of the synchronous circular centred-orbit motion is only valid under some special situations. In practice, the centralizing spring, which centralizes the journal in the static state, does not guarantee the motion of the journal and rotor always is a synchronous circular centred-orbit motion around the static undeformed line in the dynamic state due to the non-linear oil film forces. In order to investigate the non-linear behaviour of the rotor system, the most general method is to numerically integrate the equations of motion of the system for a given steady state rotational speed and a set of system parameters. Numerical integration method takes a longer computing time, but does not make any assumption about the motion of the journal, therefore it is able to consider the effect of other factors, such as rotor gravity, journal initial eccentricity or misalignment, seals, complex oil film models and supply pressure, etc. Under a steady state rotational speed, letting $\omega_r=\omega$ in equations (4), (5) and $\phi_D=\tau$, one has the non-dimensional

equations of the motion of the rotor system

$$\mathbf{Z}_D'' + \frac{2\xi}{\Omega}\mathbf{Z}_D' + \frac{1}{\Omega^2}(\mathbf{Z}_D - \mathbf{Z}_B) = U\,\mathrm{e}^{\mathrm{i}\tau}, \tag{18}$$

$$\mathbf{Z}_B'' + \frac{1}{2\alpha\Omega^2}(\mathbf{Z}_B - \mathbf{Z}_D) + \frac{k}{2\alpha\Omega^2}\mathbf{Z}_B = \frac{2B}{\Omega}(f_x + \mathrm{i}f_y). \tag{19}$$

These coupled non-linear differential equations can be solved by numerical integration methods. Although some fast convergence integration methods can be used [14], no one method is universally fast for every speed. Therefore, a fourth order Runge–Kutta method with a constant time step is used here. The time step for the numerical integration generally is $2\pi/400$ or $2\pi/800$, which is so small that there is no visual difference in the steady state orbits of the rotor system even if the step size is further decreased. The time series data of the first 100 cycles of the rotor system at each steady state rotational speed is not used for dynamic behaviour investigation in order to ensure that all transient motion caused by the initial conditions has decayed. The integrating results in the next 50 cycles are output as the steady state response of the rotor system at this rotational speed. If the motion of the rotor system is synchronous, the integration results in the next five integrating cycles will be the steady state response. This is automatically checked in the program by analysing the motion orbit of the rotor system.

2.2.3. *Slow acceleration method*

When the rotor is subjected to a constant acceleration, letting $\omega_r = \omega_{cr}$ in equations (4), (5), the equations of motion of the rotor system are:

$$\mathbf{Z}_D'' + 2\xi\mathbf{Z}_D' + (\mathbf{Z}_D - \mathbf{Z}_B) = U\phi_D'^2\,\mathrm{e}^{\mathrm{i}\phi_D} - \mathrm{i}U\phi_D''\,\mathrm{e}^{-\mathrm{i}\varphi_D}, \tag{20}$$

$$\mathbf{Z}_B'' + \frac{1}{2\alpha}(\mathbf{Z}_B - \mathbf{Z}_D) + \frac{k}{2\alpha}\mathbf{Z}_B = 2B(f_x + \mathrm{i}f_y), \tag{21}$$

where $\phi_D'' = \lambda = \text{constant}$ is the acceleration rate, $\phi_D' = \lambda\tau + \Omega_S$ and $\phi_D = \frac{1}{2}\lambda\tau^2 + \Omega_S\tau + \phi_{DS}$. Ω_S and ϕ_{DS} are, respectively, the steady state initial rotational speed ratio and the disc attitude angle when starting to accelerate.

The transient response of the rotor system in the acceleration process can be obtained by numerically integrating equations (20) and (21) for different system parameters and angular acceleration rates λ. In order to avoid numerical divergence in the calculation due to $\varepsilon_B > 1{\cdot}0$ which is caused by a larger integration step, the variable time step in the integration [15] is used and controlled by keeping a constant angular increment for each step. The angular increment used in the calculation generally is $\frac{1}{500}$ revolution in which numerical divergence does not appear. The effect of the integration step on calculating results was checked by varying the angular increment to as small as $\frac{1}{1000}$ revolution in order to reduce the effect of the rotor acceleration on the results.

The steady state response for the rotational speed in which the rotor starts to accelerate is taken as the initial conditions for the integration procedure. The integration procedure continues up to the given maximum rotational speed.

3. NUMERICAL RESULTS AND DISCUSSION

3.1. SOLUTION OF SYNCHRONOUS CIRCULAR CENTRED-ORBIT MOTION

There are many kinds of response curves with the multiple solution obtained by the steady state synchronous circular centred-orbit motion solution, but they all consist of three

basic forms of the multiple solutions. The variations of the ε_{BO}, ϕ_{BO}, ε_{DO} and ϕ_{DO} with the rotational speed ratio Ω for the three basic forms of the multiple solutions are shown in Figure 2 respectively. For clarity, the different scales are used in figures of $\varepsilon_{DO} - \Omega$. The arrows in Figure 2 show the jumping direction of the rotor during the increasing rotational speed. The solid lines stand for the stable solutions and the dotted line for the unstable solution.

The multiple solutions in Figures 2(a) and 2(b) are called the resonant multiple solutions, which appear between the flexible critical speed and the rigid critical speed of the flexible rotor system. As the rotational speed of the rotor system increases from the sub-critical speed region, the vibration amplitude of either the disc or the journal will increase, and not reduce even if the rotor has passed through the flexible critical speed. The relative phase angle of the disc between the disc imbalance force vector and the disc displacement vector is less than 100° before the jump appears. As soon as the rotational speed increases to a certain value, the vibration amplitude suddenly reduces and the disc relative phase angle approaches 180° which means that the disc imbalance force vector is out of phase with the disc displacement vector, i.e., the transposition of the gravity centre of the disc appears. Once the rotational speed is above the rigid critical speed, the resonant multiple solution will disappear completely. The resonant multiple solutions can also be divided into the *flexible resonant multiple solution*, which appears just above the flexible critical speed of the flexible rotor system and ends far below the rigid critical speed of the flexible rotor system, and the *rigid resonant multiple solution*, which ends very close to the rigid critical speed of the flexible rotor system respectively. The rigid critical speed of the flexible rotor system is the pin–pin critical speed when both ends of the flexible rotor are mounted rigidly; the flexible critical speed of the flexible rotor system is the translational critical speed when both ends of the flexible rotor are mounted on the centralizing springs. By using a perturbation method as in reference [3], it is shown that the largest and smallest solutions shown in solid lines are stable and the medium one shown in dotted line is unstable.

It is clear that the closer to the rigid critical speed the upper boundary speed of the flexible resonant multiple-solution speed region, the higher the disc vibration amplitude. For the rigid resonant multiple solution, the disc vibration amplitude will dramatically increase near the rigid critical speed, and the rotor has great difficulty in passing through its rigid critical speed. This is the reason why most research work has been focused on the rigid resonant multiple solution.

The multiple solution shown in Figure 2(c) is called the *isolated bifurcation multiple solution*. The isolated bifurcation multiple solution also appears in the range of rotational speeds between the flexible critical speed and the rigid critical speed of the flexible rotor system. If the rotor system can jump to the isolated bifurcation multiple solution, sudden change of the vibration amplitude and the transposition of the gravity centre of the disc will also occur at the same time. The reasons for the occurance of the isolated bifurcation multiple solution are that the dynamic characteristics of the oil film force of the squeeze film damper behave with a high level of non-linearity with a hardening characteristic in the region of high journal eccentricity ratios and that the exciting force is directly proportional to the square of the exciting frequency (i.e., rotational frequency of the rotor). The isolated bifurcation multiple solution cannot coexist with the rigid resonant multiple solution.

The variation of the rotor vibration amplitudes in both the journal and the disc positions with the rotational speed for either the resonant or the isolated bifurcation multiple solutions is very similar, both jump from a larger solution to a smaller one or vice versa. However, there is another multiple solution shown in Figure 2(d), which is called here the *swallowtail multiple solution* and which occurs in the region of the second rigid critical speed of the flexible rotor system. For the swallowtail bifurcation multiple solution, the variation

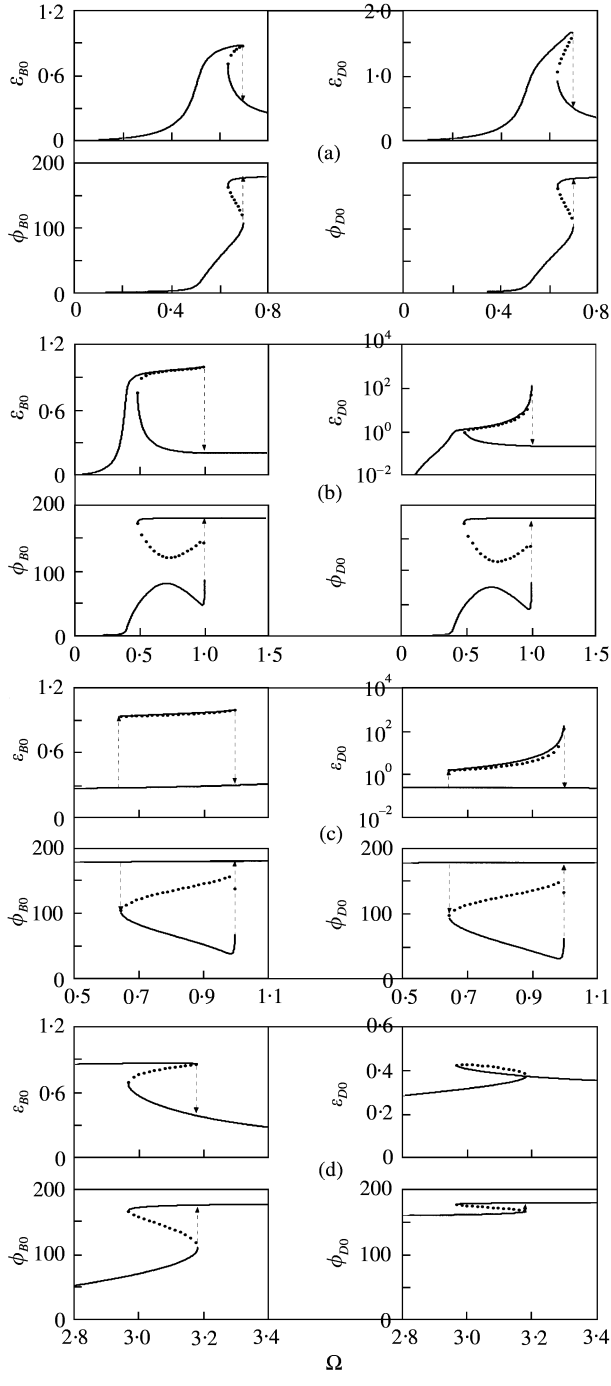

Figure 2. The basic forms of multiple solutions in the rotor system: (a) flexible resonant multiple solution ($\xi = 0{\cdot}0005$, $\alpha = 0{\cdot}10$, $k = 0{\cdot}05$, $B = 0{\cdot}05$, $U = 0{\cdot}20$) (b) rigid resonant multiple solution ($\xi = 0{\cdot}0005$, $\alpha = 0{\cdot}10$, $k = 0{\cdot}25$, $B = 0{\cdot}01$, $U = 0{\cdot}20$) (c) isolated bifurcation multiple solution ($\xi = 0{\cdot}0005$, $\alpha = 0{\cdot}10$, $k = 0{\cdot}01$, $B = 0{\cdot}025$, $U = 0{\cdot}30$); and (d) swallowtail multiple solution ($\xi = 0{\cdot}0005$, $\alpha = 0{\cdot}10$, $k = 0{\cdot}01$, $B = 0{\cdot}025$, $U = 0{\cdot}30$). Key for multiple solutions: ——, stable solutions and ●●●●●●, unstable solutions. The arrows are the jumping direction for increasing rotational speed.

of journal vibration amplitude with the rotational speed ratio is the same as that of the resonant multiple solution, the largest and smallest solutions are stable and the medium one is unstable, but the variation of the disc vibration amplitude is completely different, the largest solution in the disc response curve is always unstable, the smallest and medium solutions are stable. Therefore, the journal vibration will jump down from a larger solution to a smaller one on increasing rotational speed and jump up from a smaller one to a larger one on decreasing rotational speed, but the disc vibration is almost unchanged for increasing rotational speed as the disc is located at the node position of the second rigid model and jumps down from a larger solution to a smaller one for decreasing rotational speed. While the vibration amplitude of the rotor jumps, the change of the disc relative phase angle is small, which means that no transposition of the gravity centre of the disc happens. The swallowtail multiple solution was observed in experiments by Zhu [16].

Generally, the imbalance responses with multiple solution are a combination of these four basic types shown above. Some typical imbalance response curves with multiple solutions are shown in Figure 3.

For rotor system with many degrees of freedom and using the complex oil film model, the main problems for the synchronous circular centred-orbit motion solution are how to translate the motion equation of the rotor system to a set of non-linear algebraic equations and how to find the complete solution of the multiple-variable algebraic equations, even if the set of non-linear algebraic equations can be obtained.

3.2. STEADY STATE SOLUTION BY NUMERICAL INTEGRATION METHOD

In order to compare with the solutions of the synchronous circular centred-orbit motion, the steady state imbalance responses obtained by the numerical integration method in increasing and decreasing rotational speed with the same parameters as in Figure 2 are

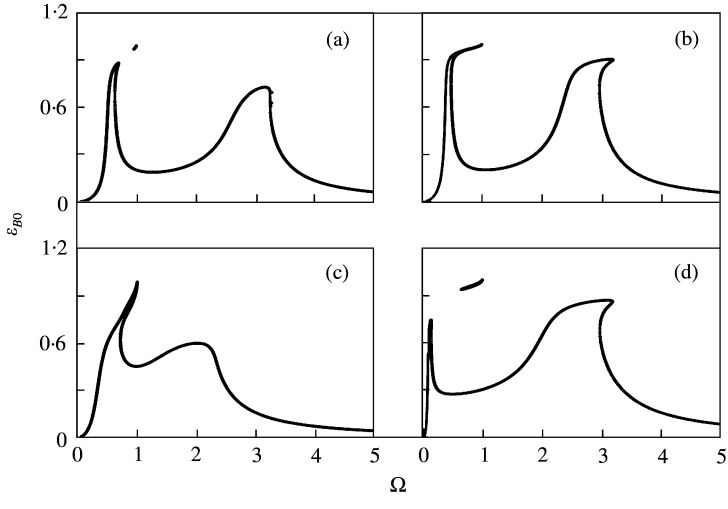

Figure 3. Typical combinations of the basic forms of the multiple solution: (a) case (1) with a flexible resonant and an isolated bifurcation multiple solution ($\xi = 0{\cdot}0005$), $\alpha = 0{\cdot}10$, $k = 0{\cdot}05$, $B = 0{\cdot}05$, $U = 0{\cdot}20$; (b) case (2) only with a rigid resonant multiple solution ($\xi = 0{\cdot}0005$, $\alpha = 0{\cdot}267$, $k = 0{\cdot}287$, $B = 0{\cdot}145$, $U = 0{\cdot}45$; (c) case (3) with a rigid resonant and a swallowatail multiple solutions ($\xi = 0{\cdot}0005$, $\alpha = 0{\cdot}10$, $k = 0{\cdot}25$, $B = 0{\cdot}01$, $U = 0{\cdot}20$; (d) case (4) with an isolated bifurcation and a swallowtail multiple solutions ($\xi = 0{\cdot}0005$, $\alpha = 0{\cdot}10$, $k = 0{\cdot}01$, $B = 0{\cdot}025$, $U = 0{\cdot}30$).

shown in Figure 4. In Figure 4, the dotted lines stand for the synchronous circular centred-orbit solutions and the solid lines for the steady state numerical integration solutions for the increasing rotational speed ($+ \Delta\Omega$, upper) or for the decreasing rotational speed ($- \Delta\Omega$, lower). It should be noted that increasing or decreasing the rotational speed just means that the rotational speed varies step by step, the changing ratio of the rotational speed is zero, i.e., $\Omega_2 = \Omega_1 \pm \Delta\Omega$.

Many numerical results show that it is very difficult to obtain all possible solutions for a given rotational speed by the numerical integration method, even if the region of the initial conditions is known [10]. In fact, the regions of the displacement and the attitude angle of

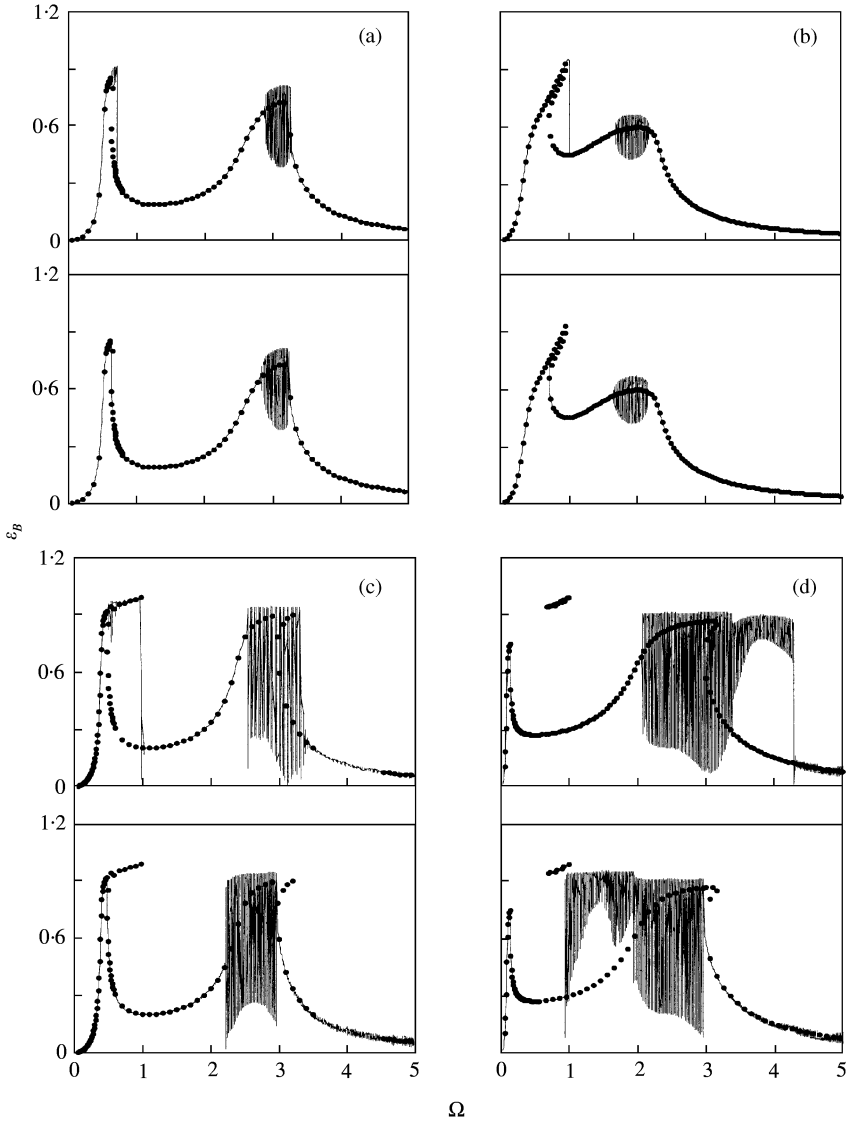

Figure 4. Steady state responses obtained by the numerical integration method for increasing rotational speed ($+ \Delta\Omega$, upper) and decreasing rotational speed ($- \Delta\Omega$, lower) for (a) case (1), (b) case (2), (c) case (3) and (d) case 4. Key for responses ●●●●●●●, for the synchronous circular centred-orbit solution; ——, for the steady state solutions by the numerical integration method. The rotor parameters in cases (1)–(4) are the same as in Figure 3.

the journal are known, but the regions of the velocity of the journal and the whirling speed of the journal are unknown. Therefore, several techniques can be used in order to make the integration result converge to different solutions. Many numerical simulations show that when the rotational speed of the rotor system is increased or decreased step by step, the final steady state variables at a given rotational speed are used as the initial conditions of the integration for the next rotational speed, which is a very efficient method to obtain multiple solutions and to save computing time. There probably exist more multiple-solution speed regions which the integration method can predict, but when the multiple solutions are found by a numerical integration method, the multiple solutions at least exist in these rotational speed regions.

If the motion of the rotor system is synchronous, there is not difference between the solution of the synchronous circular centred-orbit motion and the steady-state solution obtained by the numerical integration method.

It is obvious that there exist two different motion states at some regions of the rotational speeds, by comparing the imbalance responses for increasing and decreasing rotational speed in Figure 4. The orbits of the rotor system in the multiple-solution speed regions are not always synchronous, as subsynchronous and super-subsynchronous or almost-periodic orbits may exist. Within the multiple-solution rotational speed regions, the rotor system could run in the larger orbit or the small one, depending on whether the rotational speed of the rotor system is increased or decreased. The unstable motion state that exists between the two stable orbits and was found by the synchronous circular centred-orbit solution is not determined by the numerical integration method. The multiple-solution regions predicted by the synchronous circular centred-orbit solution can also be obtained by the numerical integration method except for the isolated bifurcation multiple solution, but the numerical integration method can also obtain the region of the multiple solution in which the motion of the rotor is non-synchronous. The numerical integration method is able to analyse the non-synchronous, almost-periodic and even chaotic motions besides the synchronous circular centred-orbit motion, and to include the effect of other factors, such as rotor gravity, initial eccentricity or misalignment of the journal, seals and the different oil film models.

Hence the synchronous circular centred-orbit motion solution is only very efficient in predicting the steady state synchronous circular centred-orbit response, but the solution of the synchronous circular centred-orbit motion is not always reliable, even if the effect of the gravity parameter is not considered, since the motions of the rotor system, in fact, are non-synchronous in some regions of the rotational speeds due to the non-linear oil film forces.

In order to show the complexity of the non-synchronous motion, a Poincaré map, often used in non-linear dynamics, can be used to eliminate the influence of the rotor's motion [17–19]. A point on the Poincaré map is referred to as the return point of the time series at a constant interval of T, where T is the sampling period. Examination of the distribution of the return points on the Poincaré map allows the nature of rotor motion to be defined. For the rotor system, when the sampling period of the Poincaré map equals the period of the exciting force, if the motion of the rotor is synchronous, subsynchronous and super-subsynchronous, then there is a set of fixed points in the Poincaré map. If the return points of the Poincaré map do not form a finite set of fixed points, but appear to fill up a closed curve, several closed (or unclosed) curves or a geometrically fractal or fuzzy structure indicates that there are more than two dominating incommensurable frequencies in the motion of the rotor system or that the motion of the rotor system is chaotic.

Figure 5 shows journal orbits (X_B, Y_B) in the multiple-solution region, corresponding power spectra of the vertical journal displacement X_B obtained using the fast Fourier transform

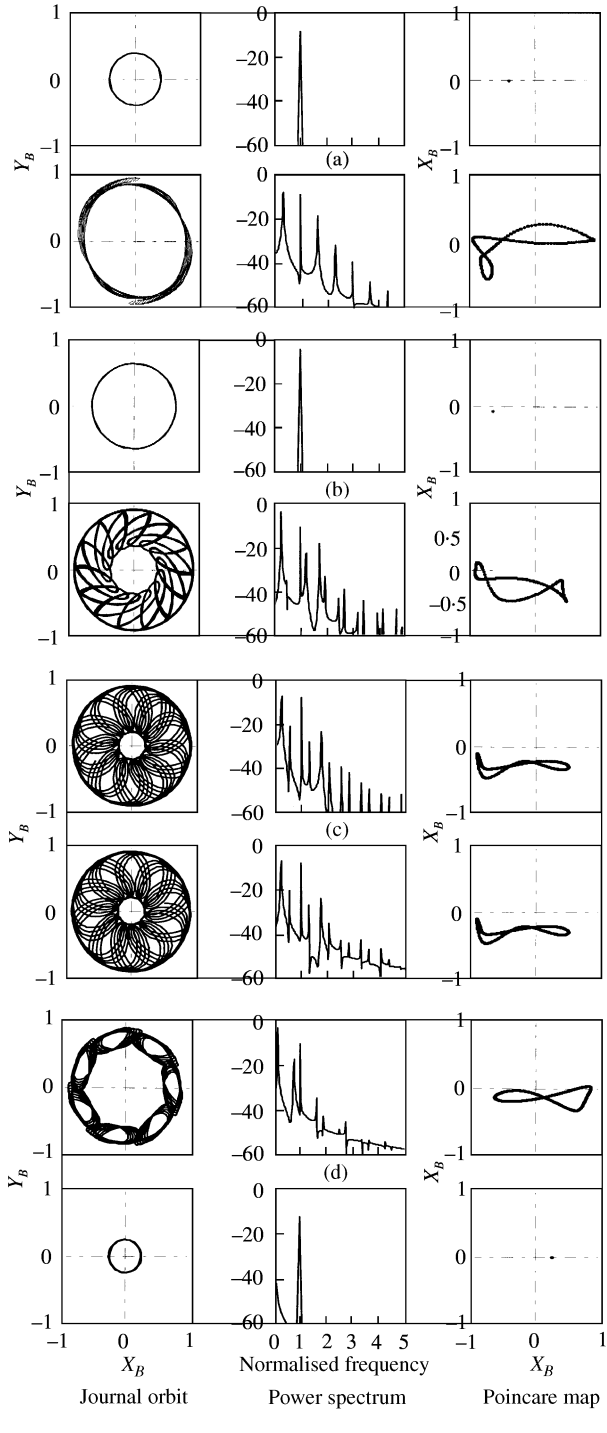

Figure 5. Journal orbit (X_B, Y_B), spectrum of journal vibration X_B and Poincaré map of (X_B, X'_B) in multiple solution region ($\xi = 0{\cdot}0005$, $\alpha = 0{\cdot}10$, $K = 0{\cdot}01$, $B = 0{\cdot}025$, $U = 0{\cdot}3$) for (a) $\Omega = 1{\cdot}5$; (b) $\Omega = 2{\cdot}0$; (c) $\Omega = 2{\cdot}5$; and (d) $\Omega = 3{\cdot}5$. In each case the upper row records increasing rotational and the lower row decreasing rotational speed.

and Poincaré maps of (X_B, X'_B). The upper row of every case shows the journal orbit, power spectrum and Poincaré map for increasing rotational speed ($+\Delta\Omega$) and the lower row shows for decreasing rotational speed ($-\Delta\Omega$). The frequency axis of the power spectrum plot was normalized using the rotor rotational frequency. In calculating the Poincaré maps, the sampling period is equal to the period of rotor rotation. For the synchronous motions, there is only one frequency component in the power spectra plots and one fixed return point in the Poincaré maps. For the non-synchronous motions, there are many frequency components in the power spectra plots and one closed curve in the Poincaré maps. It is clear that the motion of the rotor system with increasing rotational speed is synchronous, synchronous, almost 1/11-order subsynchronous (may be almost-periodic) and almost 1/8-order subsynchronous at $\Omega = 1{\cdot}5$, $2{\cdot}0$, $2{\cdot}5$ and $3{\cdot}5$, respectively, but at the same rotational speeds, the orbits of the rotor system with decreasing rotational speed are almost 1/3-order subsynchronous, almost 1/15-order subsynchronous, almost 1/11-order subsynchronous and synchronous respectively.

Generally speaking, the orbits of the rotor motion are very complex almost-periodic, and the sybsynchronous or super-subsynchronous orbits only can appear at particular rotational speeds. In most cases, the whirling speed of the rotor motion in the non-synchronous regions is neither a fraction nor an integer multiple of the rotational speed. The ratio of the whirling frequency to the rotational frequency is a very complex irrational number. It is impossible to accurately obtain the irrational number of simply analysing the whirling frequency and the rotational frequency in the power spectrum plot of the vibration signals. For example, one can obtain the whirling frequency and the rotational frequency in the spectrum plot of the rotor displacements or velocities and determine the irrational number in Figure 5 by use of an irrational approximation function, between two frequencies in MATLAB, the irrational numbers in Figure 5 are 1, 1, 6/25 and 3/25 with increasing rotational speed, 17/50, 6/25, 6/25 and 1 with decreasing rotational speed, respectively. However, the irrational numbers obtained cannot completely express the characteristics of the rotor motion. The reasons for this are: (1) The motions of the rotor system with same irrational approximation 6/25 at $\Omega = -2{\cdot}0$ and $-2{\cdot}5$ with decreasing rotational speed are completely different. (2) For the m/n-order super-subsynchronous motion, if the sampling period of the Poincaré map is n times the period of the rotor rotation, the return points of the Poincaré map should be of a finite set of m fixed points. But, for the Poincaré map in which the sampling period is 25 times the period of the rotor rotation at $\Omega = -1{\cdot}5$ and $-2{\cdot}5$, the return points of the Poincaré map still form a closed curve, not a finite set of six fixed points. (3) The mp/np-order super-subsynchronous motion and the m/n-order super-subsynchronous motion have the same irrational number, but the motions are different in view of rotordynamics [19]. In case of the m/n-order super-subsynchronous motion, a closed orbit will be formed after m whilring cycles and n rotational cycles, whereas in the case of the mp/np-order super-subsynchronous motion, a closed orbit will be formed after mp whirling cycles and np rotational cycles. The Poincaré maps in Figure 5 show that the non-synchronous motions of the rotor system are, in fact, almost-periodic.

Since the almost-periodic motions with a closed curve in the Poincaré map have different orders and motion characteristics, it is necessary to distinguish the order of the almost-periodic motion of the rotor system. Analyzing the developing process of the closed mapping curve, it is possible to determine the basic order of the almost-periodic motion. For example, the closed mapping curves in Figure 5 at $\Omega = -1{\cdot}5$ for the decreasing rotational speed and at $\Omega = +3{\cdot}5$ for the increasing rotational speed consist of three and eight moving return points marked by a set of dotted points in Figure 6. Because n points in Poincaré map often stand for 1 n-order subsynchronous motions, the n moving return points basically mean that the motion of the rotor system is processing subsynchronous

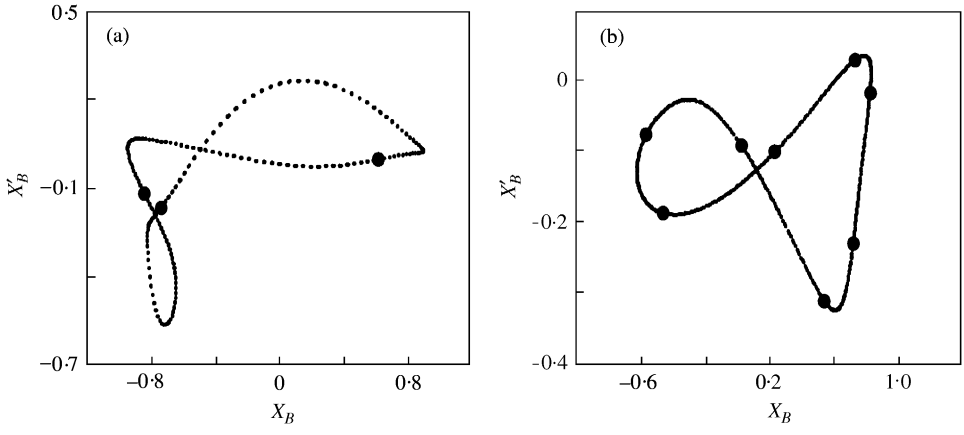

Figure 6. Formation of the Poincaré map with a closed curve. (a) for $\Omega = -1{\cdot}5$ at decreasing rotational speed and (b) for $\Omega = +3{\cdot}5$ at increasing rotational speed. The rotor parameters are the same as in Figure 5.

motions with approximate $1/n$-order. The processing frequency is so low that it cannot be found by using an FFT analyser in most real experiments and theoretical analyses, only the $1/n$-order subsynchronous frequency, called the whirling frequency here, can be observed in the power spectra. In fact, the complex almost-periodic motions in Figure 5 at $\Omega = -1{\cdot}5$ and $+3{\cdot}5$ are formed by processing of simple 1/3 or 1/8-order sub-synchronous orbits at a very slow processing frequency respectively.

For the almost-periodic $1/n$-order subsynchronous motions, there should exist at least three frequency components in the rotor motion, i.e., a rotor rotational frequency, an approximate $1/n$-rotational whirling frequency and a very slow processing frequency of the whole subsynchronous orbit. The power spectrum of the almost-periodic rotor motion should consist of a $1/n$-order subharmonic whirling frequency, a rotor rotational frequency, a low processing frequency and their multiple components and combinations due to non-circular motion orbit and the interaction between these frequencies. It is difficult to analyse the complexity of the almost-period motion only by the spectrum analysis due to the large number of frequency components. The combination of information from the rotor orbit, spectrum and Poincaré map is essential to thoroughly understand the complexity of the almost-periodic motion.

The reason for the multiple solutions and the non-synchronous motions occurrance is that the oil film forces produced by the squeeze film damper are highly non-linear in the region of the high journal eccentricity ratios; the static initial eccentricity or the misalignment of the journal discussed by Zhao *et al.* [17, 18] makes the non-linearity more serious but is not the real reason.

Although the harmonic balance method [6, 7], trigonometric collocation method [8] and generalized polynomial expansion method [9] are used successfully to analyze the characteristics of non-linear dynamic systems, one must taken care if they are applied to analyze the dynamics of the rotor systems with non-linear squeeze film dampers. Since the motion of a rotor system with squeeze film dampers is often almost-periodic, it is impossible to know the order of the subsynchronous or super-subsynchronous orbits in advance and where the subsynchronous or super-subsynchronous orbit occurs, and which frequency components should be considered in the approximate analyses. This may be the reason why these methods have not been widely used yet to predict the multiple solutions in the rotor systems with squeeze film dampers.

3.3. SLOW ACCELERATION SOLUTION

In the case without the gravity effect, the vibration amplitudes of both the journal and disc positions in the slow acceleration process can be expressed by the journal and disc eccentricity.

Comparison of the imbalance responses determined by the slow acceleration method for both acceleration and deceleration for the same parameters as in Figure 3 with the synchronous circular centred-orbit solutions are shown in Figure 7. In Figure 7, the dotted lines stand for the synchronous circular centred-orbit solutions and the solid lines for the slow acceleration solutions in the accelerating speed ($\lambda = +0{\cdot}0005$) or decreasing speed

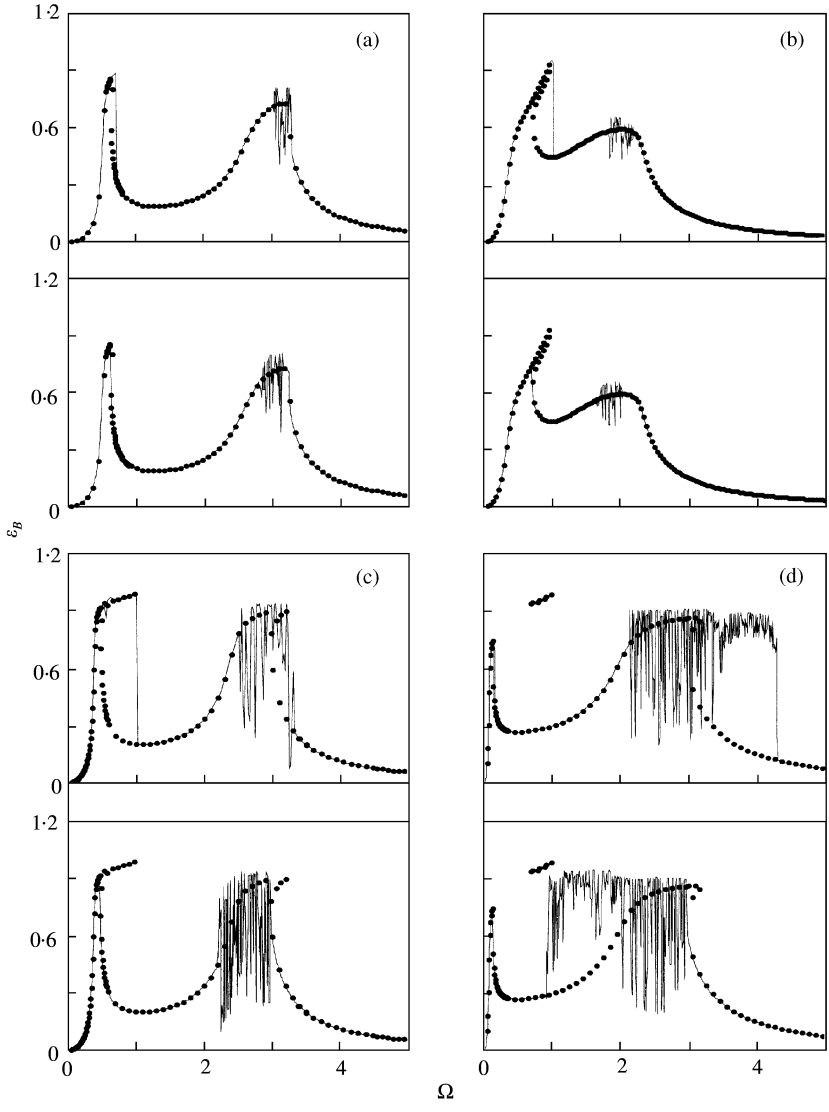

Figure 7. Comparison of imbalance responses obtained by the slow acceleration method and by the synchronous circular centred orbit solution for (a) case (1), (b) case (2), (c) case (3); and (d) case (4). Key: ·····, synchronous circular centred orbit solution and ——, slow acceleration solution. The rotor parameters in cases (1)–(4) are the same as in Figure 3, with the upper figures in each case recording the acceleration solution ($+\lambda$) and the lower figure the acceleration solution ($-\lambda$).

($\lambda = -0{\cdot}0005$) operations. It is clear that the results from the slow acceleration method are in very good agreement with the synchronous circular centred-orbit solutions in the speed regions of synchronous motion except for the isolated bifurcation multiple solution.

Comparison of the imbalance responses determined by the slow acceleration method and by the steady state numerical integration solutions with the same system parameters is shown in Figure 8. The results obtained by the slow acceleration method are also in very good agreement with the steady state solutions obtained by the numerical integration method. The slow acceleration method can predict not only the synchronous multiple-solution regions, but also the non-synchronous multiple-solution regions. Due to the rotor acceleration (or deceleration) effect, the starting and the end speeds of the multiple-solution speed region will move slightly towards the high (or low) rotational speed, which can be

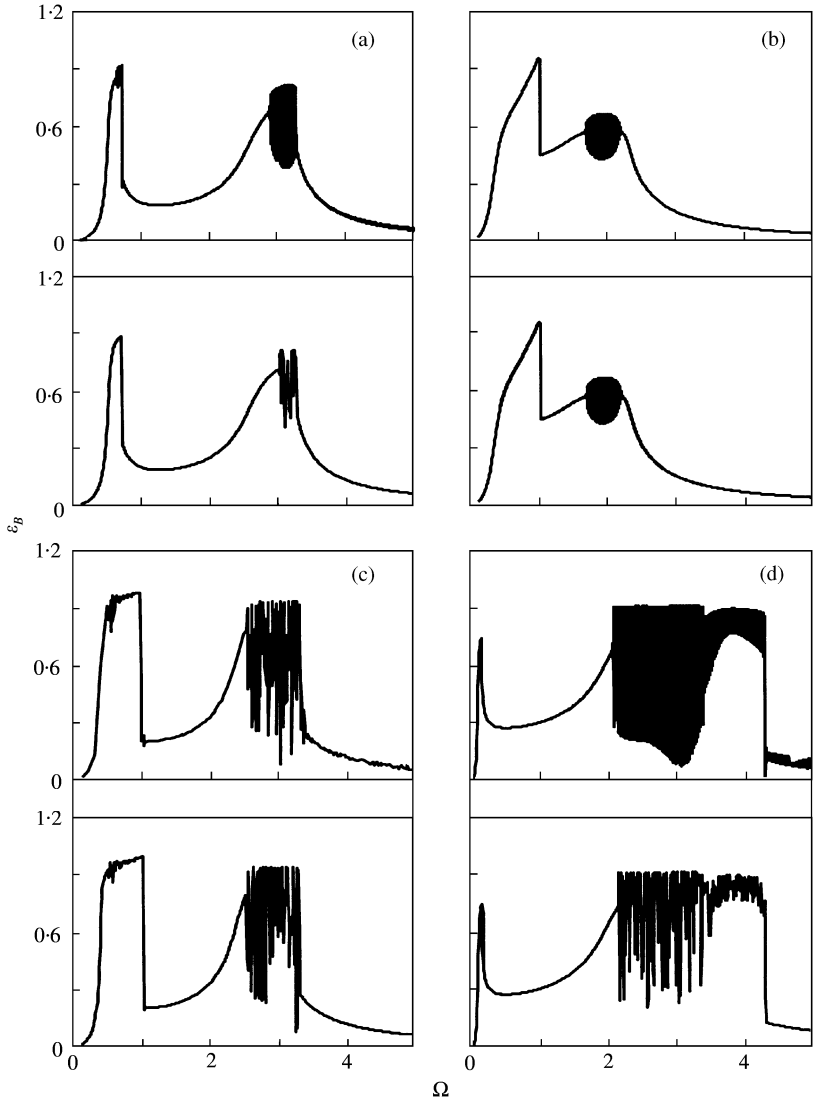

Figure 8. Comparison of the imbalance responses calculated by numerical integration method (+ $\Delta\Omega$, upper) and slow acceleration method (+ λ, lower) for (a) case (1); (b) case (2); (c) case (3); and (d) case (4). The rotor parameters in cases (1)–(4) are the same as in Figure 3.

minimized by decreasing the angular acceleration ratio used in the slow acceleration calculation.

Since the rotor motion during acceleration or deceleration is a non-stationary process with time varying frequency, the short-time Fourier transform (STFT) [20] may be used to analyze the frequency content of the non-stationary motion. Using the STFT and directional spectrogram, one can locate where the non-synchronous motion occurs and what frequencies there are in the rotor motion and hence obtain almost the same power spectrum as in Figure 5. When the STFT is used, equal-time steps in the slow acceleration analysis should be used.

Similarly, the slow acceleration method can also be used to consider many effects, such as the gravity, journal initial eccentricity or misalignment, seals, oil film models and supply pressure, etc. A major advantage of this method is that it can save computing time in comparison with the numerical integration method and predict the non-synchronous motion region of the rotational speeds with the synchronous circular centred-orbit solution. For rotor systems with many degrees of freedom, the transient properties transfer approach (TPTA) [21], successive merging and condensation (SMAC) [22] and others can be used to develop an efficient and reduced computing time method for the acceleration process.

4. CONCLUSIONS

The behaviour of the multiple-solution response in a flexible rotor supported on two identical squeeze film dampers with a centralizing spring is studied by the synchronous circular centred-orbit motion solution, numerical integration method and slow acceleration method under the assumption of the short bearing and cavitated oil film, the differences of computational results by three methods are compared. It is shown that there are many non-linear phenomena in the rotor system with squeeze film dampers including regions of multiple-solution response. The reason is that the oil film forces produced by the squeeze film damper are highly non-linear in the region of the high journal eccentricity ratios. There are three basic forms for the multiple-solution response in the flexible rotor-squeeze film damper system, which are resonant multiple solution, isolated bifurcation multiple solution and swallowtail multiple solution. In the multiple solution speed regions, the rotor motion may be subsynchronous, super-subsynchronous and almost-periodic, besides synchronous motion. Therefore, the assumption of synchronous circular centred-orbit motion can only be used in special cases even if the effect of gravity on the rotor system is not included. The steady state numerical integration method is very useful, but time-consuming. The slow acceleration method can predict not only the multiple-solution speed regions, but also the non-synchronous response regions. Both the numerical integration method and the slow acceleration method can be used to consider the effect of other factors, such as the seals, journal misalignment and initial eccentricity, gravity, oil supply groove and oil film models. The most effective process is to first determine the basic regions of the multiple solution and the non-synchronous motion by using the slow acceleration method, then to analyze in detail the non-linear behaviour of the system using the numerical integration method if necessary.

ACKNOWLEDGMENT

The authors gratefully acknowledge the partial support of the European Community in the scope of the BRITE/EURAM program under contract BRPR-CT97-0544 IMPACT project.

REFERENCES

1. L. M. GREENHILL and H. D. NELSON 1982 *Journal of Mechanical Design* **104**, 334–338. Iterative determination of squeeze film damper eccentricity of flexible rotor systems.
2. L. J. MCLEAN and E. J. HAHN 1983 *Journal of Lubrication Technology* **105**, 22–28. Unbalance behaviour of squeeze film damped multi-mass flexible rotor bearing systems.
3. L.J. MCLEAN and E. J. HAHN 1983 *Journal of Tribology* **107**, 402–409. Stability of squeeze film damped multi-mass flexible rotor bearing systems.
4. D. L. TAYLOR and B. R. K. KUMAR 1983 *Journal of Engineering for Power* **105**, 551–559. Close-form, steady-state solution for the unbalance response of a rigid rotor in squeeze film damper.
5. G. MENG and Z. Q. XUE 1985 *ASME* 85-*DET*-141. Investigation on steady-state response and its non-linear characteristics of flexible rotor-squeeze film damper system.
6. T. N. SHIAU and J. L. HWANG 1993 *Journal of Engineering for Gas Turbines and Power* **115**, 218–226. A study on stability and response analysis of a non-linear rotor system with mass unbalance and side load.
7. M. C. LEVESLEY and R. HOLMES 1994 *Proceedings of Institution of Mechanical Engineers, Part. G* **208**, 41–51. The efficient computation of the vibration response of an aero-engine rotor-damper assembly.
8. A. N. JEAN and H. D. NELSON 1990 *Journal of Vibration and Sound* **143**, 473–489. Periodic response investigation of large non-linear rotordynamic system using collocation.
9. J. L. HWANG and T. N. SHIAU 1991 *Journal of Vibration and Acoustics* **113**, 299–308. An application of the generalized polynomial expansion method to non-linear rotor bearing systems.
10. D. L. TAYLOR and B. R. K. KUMAR 1980 *Journal of Lubrication Technology* **102**, 51–58. Non-linear response of short squeeze film dampers
11. R. A. COOKSON and S. S. KOSSA 1980 *International Journal Mechanical Science* **22**, 313–324. The effectiveness of squeeze film damper bearings supported flexible rotors without a centralizing spring.
12. R. HOLMES 1972 *Journal of Mechanical Engineering Science* **14**, 74–77. The non-linear performance of squeeze film bearings.
13. J. F. BOOKER 1965 *Journal of Basic Engineering* **87**, 533–535. A table of the journal bearing integral.
14. F. L. CHU and R. HOLMES 1998 *Computation Methods Applied Mechanics and Engineering* **164**, 363–373. Efficient computation on non-linear response of a rotating assembly incorporating the squeeze-film damper.
15. C. S. ZHU *Proceedings of the Fifth International Symposium on Transient Phenomena and Dynamics of Rotating Machinery*, Honolulu, Hawaii, 210–221. Acceleration characteristics of a flexible rotor system supported on non-linear squeeze film damper.
16. C. S. ZHU 1994 *Journal of Zhejiang University* **28**, 132–140. The non-linear characteristics of a flexible rotor supported on the squeeze film dampers (in Chinese).
17. J. Y. ZHAO and E. J. HAHN 1993 *Proceedings of Institute Mechanical Engineering, Part C* **207**, 383–392. Subharmonic, quasi-periodic and chaotic motions of a rigid rotor supported by an eccentric squeeze film damper.
18. J. Y. ZHAO, I. W. LINNETT and L. J. MCLEAN 1994 *Journal of Tribology* **116**, 361–368. Stability and bifurcation of unbalance response of a squeeze film damped flexible rotor.
19. C. S. ZHU and H. ULBRICH 2000 *International Journal of Rotating Machinery* **6**, 301–312. Bifurcation behaviour of a flexible rotor supported on non-linear squeeze film dampers without centralized spring.
20. J. C. MOSS and J. K. HAMMOND 1994 *Mechanical Systems and Signal Processing* **8**, 243–258. A comparison between the modified spectrogram and the pseudo-wigner-ville distribution with and without modification.
21. R. SUBBIAH, A. S. KUMAR and T. S. SANHAR 1988 *Journal of Applied Mechanics* **55**, 448–452. Transient dynamic analysis of rotors using the combined methodologies of finite elements and transfer matrix.
22. S. RATAN and J. RODRIGUE 1992 *Journal of Vibration and Acoustics* **114**, 477–488. Transient dynamic analysis of rotors using SMAC techniques, Part 1, Formulation, Part 2. Numerical study.

APPENDIX A: NOMENCLATURE

B	bearing parameter, $B = \mu RL^3/m_B\omega_{cr}^2C^3$
C	radial clearance of the squeeze film damper

c_D	external damping coefficient at the mid-plan disc
e	eccentricity from the undeformed line
e_u	imbalance eccentricity of the disc
F_r, F_t	oil film forces in the polar co-ordinate system
F_x, F_y	oil film forces in the Cartesian co-ordinate system
$\bar{F}_x$, $\bar{F}_y$	non-dimensional oil film forces of the squeeze film damper in the Cartesian co-ordinate system
h	oil film thickness, $h = C(1 + \varepsilon_B \cos\ \theta)$
i	complex unit
I	bearing integral
k_a	stiffness of the centralizing spring
k_s	stiffness of the shaft
k	stiffness ratio, $k = k_a/k_s$
L	land length of the squeeze film damper
m_B	lumped mass as journal station
m_D	lumped mass at mid-plane disc station
p	oil film pressure
R	journal radius of the squeeze film damper
t	time
U	imbalance parameter of the rotor system, $U = e_\mu/C$
x, y, r, θ	Cartesian and polar co-ordinates
X, Y	$X = x/C$, $Y = y/C$
$\mathbf{Z}$, $\mathbf{z}$	complex variables, $\mathbf{Z} = X + \mathrm{i}Y$, $\mathbf{z} = x + \mathrm{i}y$
α	mass ratio of the rotor system, $\alpha = m_B/m_D$
θ	journal position angle measured from line of journal centres
θ_1, θ_2	angles from line of journal centres to start and end of positive pressure region
ε	non-dimensional eccentricity ratio with C, $\varepsilon = e/C$
φ	attitude angle
ϕ_D	phase angle of the disc imbalance force vector with respect to the x axial direction.
ϕ_{DO}	relative phase angle of the disc imbalance force vector with respect to the rotor disc displacement vector.
ϕ_{DS}	disc attitude angle of the starting to accelerate
λ	acceleration ratio
μ	oil viscosity
τ	non-dimensional time, $\tau = \omega_r t$
ω	rotational speed
ω_r	reference rotational speed
ω_{cr}	first pin–pin critical speed of the flexible rotor mounted rigidly, $\omega_{cr} = \sqrt{k_s/m_D}$.
Ω	rotational speed ratio, $\Omega = \omega/\omega_{cr}$
Ω_r	reference rotational speed ratio, $\Omega_r = \omega/\omega_r$
Ω_S	initial rotational speed ratio of the starting to accelerate
ξ	linear air damping ratio, $\xi = c_D/2m_D\omega_{cr}$
$'$	$\mathrm{d}/\mathrm{d}\tau$
$\cdot$	$\mathrm{d}/\mathrm{d}t$

Subscripts

B	bearing
D	disc
o	CCO solution